

## Inversion of the COPROD2 magnetotelluric data using a Diffusive-to-Propagative Mapping (DPM)

Benoît Tournerie and Dominique Gibert

Géosciences Rennes (CNRS: UPR 4661) and Université de Rennes 1, France

Jean Virieux

Institut de Géodynamique, Université de Nice Sophia-Antipolis, France

**Abstract.** Diffusive-to-Propagative Mapping (DPM) transforms a diffusive electromagnetic field into a dual wave field to produce electromagnetic reflectivity images similar to non-migrated seismic sections. An application of DPM to the COPROD2 data set gives reflectivity images showing three distinct reflectors attributed to resistivity jumps located at depths ranging from 2 to 50 km. The deeper reflector may be related to a major west-dipping seismic reflector detected with the COCORP seismic data.

### Introduction

Diffusion disables direct application of seismic imaging techniques to low-frequency electromagnetic soundings, and the seminal papers by *Zhdanov and Frenkel* [1983] and *Filatov* [1984] motivated the development of migration-like algorithms for diffusive fields. Encouraging theoretical results have since been obtained by several authors [*Lee et al.*, 1987; *Levy et al.*, 1988; *Gibert and Virieux*, 1991; *Zorgati et al.*, 1991; *Lee and Xie*, 1993; *Zhdanov et al.*, 1993; *Gibert et al.*, 1994; *Virieux et al.*, 1994; *Wilson*, 1994], and we present an application of the Diffusive-to-Propagative Mapping (DPM) [*Gibert and Virieux*, 1991; *Gibert et al.*, 1994] to the magnetotelluric COPROD2 data set [*Jones*, 1993].

DPM images the sharp gradients of electrical conductivity and allows a direct and high-resolution imaging of electromagnetic reflectivity. The link with the seismic approach is made through a Bäcklund transformation relating solutions,  $\vec{D}(\vec{x}, t)$ , of the diffusion equation to solutions,  $\vec{W}(\vec{x}, q)$ , of the wave equation [*Bragg and Dettman*, 1968; *Filippi and Frisch*, 1969; *Filatov*, 1984; *Lee et al.*, 1989]. We have,

$$\vec{D}(\vec{x}, t) = \int_0^\infty \frac{q}{2\sqrt{\pi t^3}} \exp\left(-\frac{q^2}{4t}\right) \vec{W}(\vec{x}, q) dq \quad (1)$$

where the diffusive field  $\vec{D}(\vec{x}, t)$  is either the electrical or the magnetic field and verifies the diffusion equation

$$\vec{\nabla} \times \vec{\nabla} \times \vec{D}(\vec{x}, t) + \frac{\mu}{\rho(\vec{x})} \frac{\partial}{\partial t} \vec{D}(\vec{x}, t) = 0, \quad (2)$$

while the dual the field,  $\vec{W}(\vec{x}, q)$ , obeys a wave equation

$$\vec{\nabla} \times \vec{\nabla} \times \vec{W}(\vec{x}, q) + \frac{\mu}{\rho(\vec{x})} \frac{\partial^2}{\partial q^2} \vec{W}(\vec{x}, q) = 0, \quad (3)$$

where  $\rho(\vec{x})$  is the electrical resistivity and  $\mu$  is the magnetic permeability. The ratio  $\mu/\rho(\vec{x})$  appearing in equation (3) gives a wave 'velocity',

$$c(\vec{x}) = \sqrt{\frac{\rho(\vec{x})}{\mu}}, \quad (4)$$

expressed in unit of length per square-root of physical time  $t$ . The independent variable  $q$  is a pseudo-time given in square-root of  $t$ . DPM is made by solving equation (1) in order to reconstruct the wave field  $\vec{W}$  from the diffusive field  $\vec{D}$  and to produce reflectivity sections in the  $(\vec{x}, q)$  space in a way very similar to the well-known seismic reflection images. Equation (1) can be solved either in the time,  $t$ , domain [*Lee and Xie*, 1993] or in the dual,  $\omega$ , Fourier space [*Gibert and Virieux*, 1991; *Gibert et al.*, 1994] where it reads

$$\vec{D}(\vec{x}, \omega) = \int_0^\infty \exp(-q\sqrt{i\omega}) \vec{W}(\vec{x}, q) dq. \quad (5)$$

This latter possibility is more adapted to the present purpose since magnetotelluric data are traditionally given as apparent resistivity and phase with respect to frequency [*Zhdanov and Keller*, 1994]. An issue of critical importance encountered when solving either equation (1) or (5) is the considerable ill-posedness attached to both noisy and incomplete data. Indeed, the numerical resolution of equation (5) is a very unstable inverse problem requiring much care, and a detailed numerical study indicates that fully non-linear inverse techniques like simulated annealing produce stable solutions [*Gibert et al.*, 1994]. As shown by *Donoho* [1992] the numerical inversion of integral equations with Laplace-

Copyright 1995 by the American Geophysical Union.

Paper number 95GL02016  
0094-8534/95/95GL-02016\$03.00

like kernels can be strongly regularized if the unknown solution  $\vec{W}$  satisfies some sparsity constraints. In the present study we assume that  $\vec{W}$  is a sequence of echoes reflected by the edges of the objects to detect,

$$\vec{W} = \sum_{n=1}^N \vec{W}_n \delta(q - q_n), \quad (6)$$

and the inverse problem is to estimate both the amplitudes,  $\vec{W}_n$ , and the occurrence times,  $q_n$ , of the arrivals. A detailed description of the numerical techniques used to estimate these parameters is given by *Gibert et al.* [1994].

## Analysis of the COPROD2 data set

### Presentation of the COPROD2 data

A detailed description of the magnetotelluric COPROD2 data set is given by *Jones* [1993]. The apparent resistivity and phase have been measured in the  $5.5 \times 10^{-3} - 384$  Hz frequency range. The data are available at 35 stations located along a 407 km profile almost perpendicular to the North American Central Plain (NACP) magnetic anomaly in the Williston Basin (Figure 1). Both the TM and TE modes, which correspond to a geometry where the magnetic field is respectively parallel or perpendicular to the strike of the geological structures, have been considered. In order to allow a full comparison of our results with those already obtained by other authors [*Jones*, 1993], the data used in the present study are corrected for the static shifts [*Jones*, 1988] and are shown as apparent resistivity and phase curves on Figure 2.

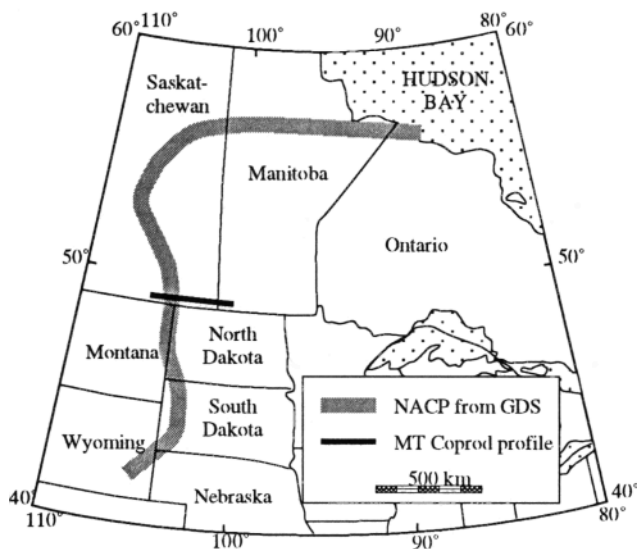


**Figure 1.** Localization of the COPROD2 magnetotelluric profile (heavy solid line). The center of the NACP magnetic anomaly is also shown (grey ribbon). Modified from *Jones and Craven* [1990].

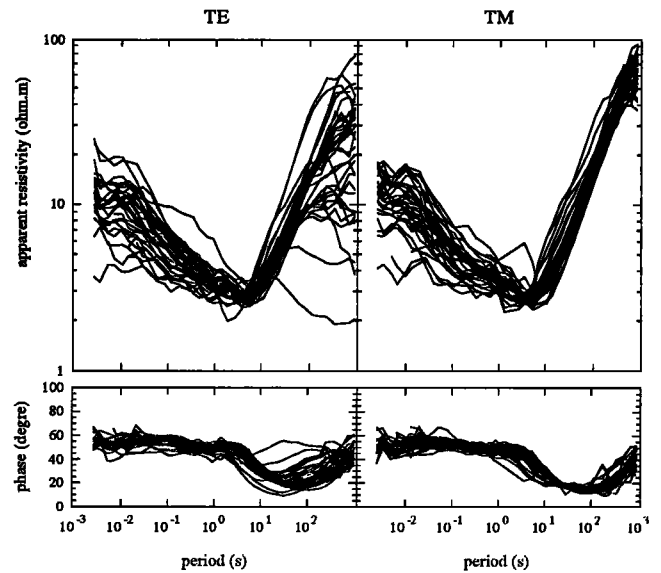


**Figure 2.** Apparent resistivity and phase curves recorded at the 35 station of the COPROD2 profile and corrected for the static shifts.

### DPM applied to the COPROD2 data set

The basic data needed to invert equation (5) are the Fourier coefficients of either the electrical field or the magnetic field. Moreover, since the time dependence of the ionospheric sources creating the magnetotelluric signals is unknown, some deconvolution is needed to obtain the Earth's electromagnetic response corresponding to an impulsive source. Fortunately, the standard processing of magnetotelluric data involves the computation of impedance functions which are implicitly deconvolved for the ionospheric source function. The only non-standard computation we applied is the transformation of both apparent resistivity,  $\rho_a(\omega)$ , and phase,  $\Phi(\omega)$ , into the diffusive response,

$$D(\omega) = \frac{\exp[i(\Phi(\omega) - \pi/4)]}{2} \sqrt{\frac{\rho_a(\omega)}{\rho_s}} - \frac{1}{2}, \quad (7)$$

where  $\rho_s$  is the electrical resistivity of the shallow layers in the Earth.  $D(\omega)$  is the diffusive impulse response corresponding to the conductive geological structures and was derived by *Levy et al.* [1988] for 1-D layered media. The same response is reasonably valid for 2-D structures as shown by the asymptotic simulations (i.e. the equivalent of ray theory for diffusion) performed by *Virieux et al.* [1994]. This response constitutes the data used to invert equation (5) and obtain the wave field  $\vec{W}$ .

The choice of a surficial resistivity,  $\rho_s$ , fixes a surficial velocity,  $c_s$ , which controls the static shifts of the reconstructed wave field. This choice is not too critical unless large unrealistic resistivities are used. Figure 3 represents *DPM* results obtained for the TM data of the westernmost station preprocessed through equation

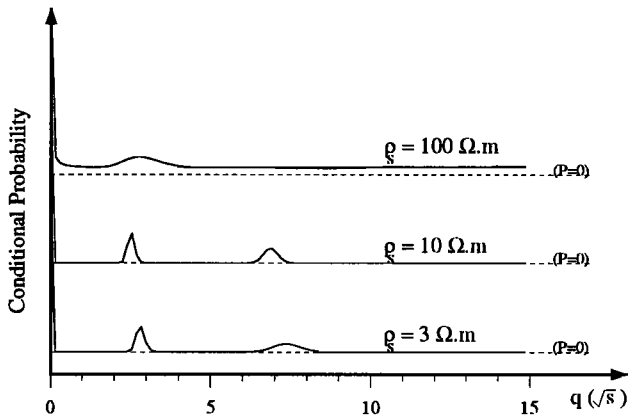


**Figure 3.** DPM inversions of the TM data for westernmost station. The three plots show the probability curves of the reflected echoes computed for different assigned values of the surface resistivity.

(7) with  $\rho_s = 3, 10,$  and  $100 \Omega.m$ . These results represent the conditional probability to have an echo at a particular pseudo-time (see *Gibert and Virieux* [1991] and *Gibert et al.* [1994] for more details). Both DPM obtained for the lower two values of resistivity are essentially identical but for a small time lag: the echoes reconstructed for  $\rho_s = 3 \Omega.m$  are late with respect to their equivalent for  $\rho_s = 10 \Omega.m$ . This observation agrees with equation (4) which shows that the larger the resistivity, the larger the velocity. A precise computation of the static shifts is intractable since it involves an integration over unknown depths for which the surficial resistivity acts. The DPM results obtained for  $\rho_s = 100 \Omega.m$  are strongly biased and only the latest echo remains, the former being now anticausal and totally delocalized (i.e. constant conditional probability along the pseudo-time axis). In the remaining, a surficial resistivity  $\rho_s = 3 \Omega.m$  corresponding to the mean resistivity obtained from laterologs performed along the profile has been used for all stations [*Jones, 1988*].

The DPM sections obtained for all 35 stations and for both the TM and TE modes are represented in Figure 4. It must be emphasized that the displayed sections were obtained by plotting together all 35 individual DPM traces (like those in Figure 3). Each inversion was performed independently from the others and no inter-trace coherency criterion was applied.

### Interpretation and discussion

Most reflections inverted from the TE data arrange themselves onto 4 reflectors labelled from 1 to 4 on Figure 4. Reflector 1 is tracked across the whole profile and is also coherently recovered from the TM data. This reflector has a rough synclinal shape with an average two-way pseudo-time of  $3\sqrt{s}$ , a shallower easternmost end with pseudo-times decreasing to  $2\sqrt{s}$ , and a deeper middle part with pseudo-times around  $4\sqrt{s}$ . Assuming

a mean resistivity of  $3 \Omega.m$  for the shallow sedimentary layers, these pseudo-times give an average depth of  $2.3 km$ , and depths of  $1.5 km$  and  $3.0 km$  for the easternmost end and the middle part respectively. This geometry is fully compatible with the shallow electrical structure derived from laterologs which evidenced a sharp increase of electrical resistivity associated with the Ashern dolomite marker [*Jones, 1988*]. Both the sharpness of reflector 1 and the coherency of the results indicate that reflector 1 can be confidently attributed to this geological interface.

Reflectors 2 and 3 are not equally recovered from the TE and TM sections. When grouped altogether, the tracked reflectors form a reflectivity ribbon crossing the whole profile with two-way pseudo-times varying from  $6\sqrt{s}$  to  $9\sqrt{s}$ . The general shape of reflectors 2 and 3 mimics the one of reflector 1 and, although the pseudo-times of the latter are not exactly half of those for the formers, it cannot be totally excluded that reflectors 2 and 3 are segments of the first multiple of reflector 1. However, we give a low probability to this possibility since our previous synthetic tests never displayed such multiples, even for much stronger reflectors than the presently discussed ones. An alternative interpretation is that reflectors 2 and 3 are primary and created by a resistivity jump with a depth ranging from  $7 km$  to  $11 km$  (assuming  $\rho = 10 \Omega.m$  below reflector 1), the shallower depths being on the easternmost wing of the profile. Such a resistivity variation may be associated with a strong seismic reflector evidenced with seismic refraction data [*Morel-à-l'Hussier et al., 1987*].

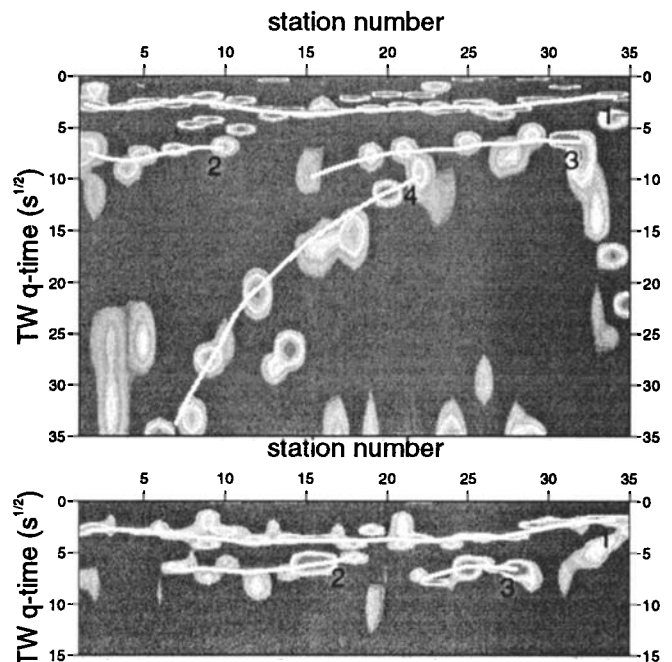


**Figure 4.** DPM electromagnetic reflectivity images obtained for the TE (top) and TM (bottom) COPROD2 data. Labelled white lines enhance the reflectors discussed in the text.

Reflector 4 is only recovered from the TE data and constitutes an alignment with a steep westward deepening. Two-way pseudo-times range from  $10\sqrt{s}$  to  $35\sqrt{s}$ . The unrecovery of reflector 4 from the TM data set illustrates the differential sensitivity between TE and TM modes to a given structure and cannot be attributed to the noise whose amount is the same in both data sets (see Figure 2). Such a discrepancy has also been observed in synthetic inversions and emphasized by Levy *et al.* [1988]. The depth range of the resistivity jumps producing reflector 4 strongly depends on the resistivities of the overlying rocks. As stated in the introduction, the magnetotelluric approximation corresponds to a seismic design which disables any kind of velocity analysis, and we must use velocities computed with resistivity estimates furnished by other inversion methods [Jones, 1993]. Although strongly dependent upon the particular inversion algorithm used, these resistivity estimates mostly fall in the  $[1, 1000] \Omega.m$  interval, with an average value of the order of  $10 \Omega.m$  (see Jones [1993] for a review). Taking this last estimate for the resistivity, we find a depth range  $[15, 50] km$  for reflector 4. Of course, these estimates are rough and more precise values could be obtained by migrating the reflectivity images of Figure 4. Let us notice however that the top of reflector 4 coincides with the low-resistivity body found by Jones [1993] and we may conjecture that the whole electromagnetic reflector fits with the west-dipping reflectivity zone found in the COCORP seismic survey performed  $100 km$  to the south of the COPROD2 profile [Nelson *et al.*, 1993].

**Acknowledgments.** We are pleased to thank Dr. Alan Jones for both his kind supplying of the high-quality COPROD2 data set and his very constructive comments. Thanks to Guy Marquis and Andrew Wilson for their comments. Processings were done with the computational facilities operated by the Centre des Ressources Informatiques from Université de Rennes 1, and we thank Jean-Pierre Boulard, François Dagorn and Eric Picheral for their skilled assistance. This study was supported by CNRS/INSU grants (DBT 'Fluides & Failles', ATP 'Tomographie').

## References

- Bragg, L.R., and J.W. Dettman, Related problems in partial differential equations, *Bull. Am. Math. Soc.*, **74**, 375-378, 1968.
- Donoho, D.L., Superresolution *via* sparsity constraints, *SIAM J. Math. Anal.*, **23**, 1309-1331, 1992.
- Filatov, V.V., Construction of focusing transformations of non-stationary electromagnetic fields, *Geol i Geofiz (Soviet Geology and Geophysics)*, **25**, 89-95, 1984.
- Filippi, P., and U. Frisch, Relation entre l'équation de la chaleur et l'équation des ondes de Helmholtz, *Comptes Rendus Acad. Sciences Paris*, **A268**, 804-807, 1969.
- Gibert, D., and J. Virieux, Electromagnetic imaging and simulated annealing, *J. Geophys. Res.*, **B96**, 8057-8067, 1991.
- Gibert, D., B. Tournerie, and J. Virieux, Superresolution electromagnetic imaging of the conductive Earth's interior, *Inverse Problems*, **10**, 341-351, 1994.
- Jones, A.G., The COPROD2 data set: Tectonic setting, recorded MT data, and comparison of models, *J. Geomag. and Geoelec.*, **45**, 933-955, 1993.
- Jones, A.G., and J.A. Craven, The North American Central Plain conductivity anomaly and its correlation with gravity, magnetic, seismic, and heat flow data in Saskatchewan Canada, *Phys. Earth Planet. Inter.*, **60**, 169-194, 1990.
- Jones, A.G., Static shift of magnetotelluric data and its removal in sedimentary basin environment, *Geophysics*, **53**, 967-978, 1988.
- Lee, S., G. McMechan, and C.L. Aiken, Phase-field imaging: the electromagnetic equivalent of seismic migration, *Geophysics*, **52**, 1678-1693, 1987.
- Lee, K.H., G. Liu, and H.F. Morrison, A new approach to modeling the electromagnetic response of conductive media, *Geophysics*, **54**, 1180-1192, 1989.
- Lee, K.H., and G. Xie, A new approach to imaging with low-frequency electromagnetic fields, *Geophysics*, **58**, 780-796, 1993.
- Levy, S., D.W. Oldenburg, and J. Wang, Subsurface imaging using magnetotelluric data, *Geophysics*, **53**, 104-117, 1988.
- Morel-A-l'Huissier, P., A.G. Green, and C.J. Pike, Crustal refraction surveys across the Trans-Hudson Orogen Williston basin of South Central Canada, *J. Geophys. Res.* **92**, 6403-6420, 1987.
- Nelson, K.D., D.J. Baird, J.J. Walters, M. Hauck, L.D. Brown, J.E. Oliver, J.L. Aliern, Z. Hajnal, A.G. Jones, and L.L. Sloss, Trans-Hudson orogen and Williston basin in Montana and North Dakota: New COCORP deep-profiling results, *Geology*, **21**, 447-450, 1993.
- Virieux, J., C. Flores-Luna, and D. Gibert, Asymptotic theory for diffusive electromagnetic imaging *Geophys. J. Int.*, **119**, 857-868, 1994.
- Wilson, A.J.S., Seismic processing of multichannel transient electromagnetic data, in *Proc. EAEG-EAPG meeting*, Vienna, Austria, 1994.
- Zhdanov, M., and M.A. Frenkel, The solution of the inverse problems on the basis of analytical continuation of the transient electromagnetic field in reverse time, *J. Geomag. and Geoelec.*, **35**, 747-765, 1983.
- Zhdanov, M., P. Traynin, and O. Portniaguine, Migration and analytic continuation in geoelectric imaging, *Soc. Expro. Geophys. 64th Meeting, extended abstract*, 357-360, 1994.
- Zhdanov, M., and G.V. Keller, *The geoelectrical methods in geophysical exploration*, Elsevier, New-York, 1994.
- Zorgati, R., B. Duchêne, D. Lesselier, and F. Pons, Eddy current testing of anomalies in conductive materials: 1. Qualitative imaging via diffraction tomography techniques, *IEEE Trans. Magn.*, **27**, 4416-4437, 1991.

B. Tournerie, and D. Gibert, Géosciences Rennes, Université de Rennes 1, Bât. 15 Campus de Beaulieu, 35042 Rennes cedex, France. (e-mail: tourneri@univ-rennes1.fr; gibert@univ-rennes1.fr)

J. Virieux, Institut de Géodynamique, Université de Nice Sophia-Antipolis, Av. A. Einstein, 06560 Valbonne, France. (e-mail: viri@mimosa.unice.fr)

(received February 14, 1995; revised June 19, 1995; accepted June 22, 1995.)